Green ammonia synthesis using CeO_2/RuO_2 nanolayers on vertical graphene catalyst via electrochemical route in alkaline electrolyte

HyungKuk Ju[a,b,*,1], Dong Han Seo [c,d,*,1], Sunki Chung[e,f,g,1], Xin Mao[h], Byeong-Seon An[i], Mustafa Musameh[j], Thomas R. Gengenbach[j], Hokyong Shon[c], Aijun Du[h], Avi Bendavid[k], Kostya (Ken) Ostrikov[h], Hyung Chul Yoon[l], Jaeyoung Lee[e,f,g] and Sarbjit Giddey[b]

[a] Hydrogen Research Department, Korea Institute of Energy Research, 152 Gajeong-ro, Yuseong-gu, Daejeon 34129, Republic of Korea.

[b] CSIRO Energy, Private Bag 10, Clayton South, Victoria 3169, Australia

[c] School of Civil and Environmental Engineering, University of Technology Sydney, P.O. Box 123, 15 Broadway, NSW, 2007, Australia

[d] Institute of Energy Materials and Devices, Korea Institute of Energy Technology (KENTECH), Naju, Republic of Korea

[e] School of Earth Sciences and Environmental Engineering, Gwangju Institute of Science and Technology (GIST), Gwangju 61005, Republic of Korea

[f] International Future Research Center of Chemical Energy Storage and Conversion Processes, GIST, Gwangju 61005, Republic of Korea

[g] Ertl Centre for Electrochemistry and Catalysis, GIST, Gwangju 61005, Republic of Korea

[h] School of Chemistry, Physics and Mechanical Engineering Queensland University of Technology Gardens Point Campus, Brisbane, QLD4001, Australia

[i] Platform Technology Laboratory, Korea Institute of Energy Research, 152 Gajeong-ro, Yuseong-gu, Daejeon 34129, Republic of Korea

[j] CSIRO Manufacturing, Private Bag 10, Clayton South, VIC 3169, Australia

[k] CSIRO Manufacturing, PO Box 218, Lindfield, NSW 2070, Australia

[1] Climate Change Research Division, Korea Institute of Energy Research, 152 Gajeong-ro, Yuseong-gu, Daejeon 34129, Republic of Korea.

* Corresponding author email: hyungkuk.ju@kier.re.kr ; dhseo@kentech.ac.kr

[1] These authors contributed equally to this work

[1] These authors contributed equally to this work

This PDF file includes:

Experimental

Figs. S1 to S12

Table S1 to S2

Experimental

Vertical graphene (VG) synthesis

The deposition of VG was carried out in a radio-frequency (RF) inductively coupled plasma chemical vapor deposition (CVD) system (shown in **Figure S8** of the Supporting Information). Ni foam (purity: > 99.99%, porosity: ≥ 95%, surface density: 346 g m^{-2}, MTI co. USA) was used as the base electrode. After loading the Ni foam into the deposition chamber, the chamber pressure was evacuated to attain a base pressure of 4.0 Pa. Then the gas mixture of Ar (10 sccm), CH_4 (20 sccm) and H_2 (10 sccm) was introduced into the chamber using mass flow controllers and constant pressure of 4.0 Pa was maintained. Then the plasma was generated at a constant power of 1000 W for 10 min to synthesize the vertical graphene on Ni foam. Vertical graphene synthesis was done in a high vacuum chamber, using a highly purified gases which makes the vertical graphene to be devoid of possible nitrogen contamination during the synthesis.[1]

RuO_2 and CeO_2 thin film deposition

After the synthesis of vertical graphene (VG), RuO_2 and CeO_2 nanoscale thin films were deposited using a custom-made magnetron sputtering system (CSIRO Manufacturing). The system was equipped with an axial turret magnetron head and power supply (AJA DCXS-750). The turret head was mounted vertically in the bottom of the vacuum system. The RuO_2 and CeO_2 target materials (purity: 99.9%) used for the film deposition. The nominal size of the sputter targets was 2 inches (50 mm) diameter and the distance between the target and the substrate was set at 60 mm. The films were deposited onto the vertical graphene coated on Ni foam. The deposition system was equipped with rotary and cryogenic pumps and a controlled gas introduction system. A base pressure of 1×10^{-4} Pa was attained in the chamber before the deposition. The high purity O_2 reactive gas and high purity Ar inert gas were introduced into the chamber. The deposition pressure could be set independently of the gas flow by adjusting a throttle valve. The deposition pressure was set 2.0 Pa and the film depositions were performed at room temperature. The RF power were set at 125 W. The deposition times varied between the two nanolayer films; 5 min for RuO_2 and 15 min for the CeO_2 film.

Material Characterizations

High-resolution field emission scanning electron microscopy (FE-SEM) images were obtained using a Zeiss Auriga microscope operated at 5 keV electron beam energy with an In Lens secondary electron detector. An energy dispersive X-ray spectroscopy (EDX; Oxford instrument) measurement was operated at 18 keV electron beam energy to obtain the elemental analysis data. Raman spectroscopy was performed using a Renishaw in via spectrometer with laser excitation at 514 nm with a spot size of ~ 2 μm. The surface chemical composition and electronic state of the electrode catalyst layer were analyzed via X-ray photoelectron spectroscopy (XPS) using an AXIS Nova spectrometer (Kratos Analytical Inc., Manchester, UK) with a monochromated Al Kα source at a power of 180 W (15 kV x 12 mA) and a hemispherical analyzer operating in the fixed analyzer transmission mode. The total pressure in the main vacuum chamber during analysis was typically between 10^{-9} and 10^{-8} mbar. Survey spectra were acquired at a pass energy of 160 eV and step size 0.5 eV. To obtain more detailed information about chemical structure and oxidation states, high resolution spectra were recorded from individual peaks at 40 eV pass energy and step size 0.1 eV, typically yielding a FWHM of < 0.8 eV for the Ag $3d_{5/2}$ peak and < 0.85 eV for the ester peak in PET during performance tests. The samples were analyzed at a nominal photoelectron emission angle of 0^{o} w.r.t. the surface normal. Since the actual emission angle is ill-defined in the case of rough surfaces as in this study (ranging from 0^{o} to 90^{o}) the sampling depth may range from 0 nm to approximately 10 nm. Data processing was performed using Casa XPS processing software version 2.3.15 (Casa Software Ltd., Teignmouth, UK). All elements present were identified from survey spectra. The atomic concentrations of the detected elements were calculated using integral peak intensities and the sensitivity factors supplied by the manufacturer. Binding energies were referenced to the C 1s peak either at 284.8 eV (adventitious carbon) or at 284.5 eV (graphene). The accuracy associated with quantitative XPS is ca. 10-15%. Precision (i.e. reproducibility) depends on the signal/noise ratio but is usually much better than 5%. The latter is relevant when comparing similar samples. To analyze the microstructure of CeO_2/RuO_2/VG electrode, transmission electron microscopy (TEM) samples were prepared using a conventional drop-casting method. The samples were investigated by analytical TEM (JEOL, JEM-ARM200F) at 200 kV equipped with a cold field-emission gun (CFEG) and an energy-dispersive X-ray spectrometer (EDS, Oxford). The distribution of CuO_2/RuO_2 film was determined by STEM-EDS. The electrochemical impedance spectroscopy (EIS; VSP, BioLogic) was further performed under potentiostatic mode at -0.6 V vs. RHE at excitation amplitude of 10 mV in the frequency range from 100 kHz to 1 Hz.

The concentration of produced NH_3 was determined by the indophenol blue method.

In brief, ammonia products (2 mL) were collected from the solution trap (100 mL, 0.05M H_2SO_4) and then mixed with 2 mL of 1 M NaOH solution containing salicylic acid (5 wt%) and sodium citrate (5 wt%). Subsequently, 1 mL NaClO (0.05 M) and 0.2 mL $C_5FeN_6Na_2O\cdot 2H_2O$ (1 wt%) were added into the above solution. After standing at room temperature for 2 hr, the UV-Vis absorption spectrum was measured at a wavelength of 675 nm. The concentration-absorbance curve was calibrated using standard NH_4Cl solution with the concentrations of 0.0, 0.1, 0.2, 0.5, 1.0 and 2.0 μg mL^{-1} in 0.05 M H_2SO_4. The fitting curve ($y = 0.0941x - 0.004$, $R^2 = 0.985$) shows good linear relation of absorbance value with NH_3 concentration.

The hydrazine was estimated by the method of Watt and Chrisp.

In addition, a possible by-product hydrazine (N_2H_4) was also determined by the method of Watt and Chrisp.[2] In brief, 5 mL electrolyte and 5 mL color reagent (5.99 g 4-(dimethylamino)benzaldehyde dissolved in 30 mL concentrated HCl and 300 mL ethanol) was mixed and placed at room temperature for 10 min. The UV-Vis absorption spectrum was measured at a wavelength of 457 nm. The concentration-absorbance curve was calibrated using standard N_2H_4 solution with the concentrations of 0.0, 0.2, 0.4, 0.6, 1.0 and 2.0 μg mL^{-1} in 0.05 M H_2SO_4. The fitting curve ($y = 1.437x - 0.028$, $R^2 = 0.99833$) shows good linear relation of absorbance value with N_2H_4 concentration. It shows that negligible amounts of hydrazine (~20 ppb level in 100 ml of 0.05 M H_2SO_4 solution) was detected during all consecutive NRR cycle tests.

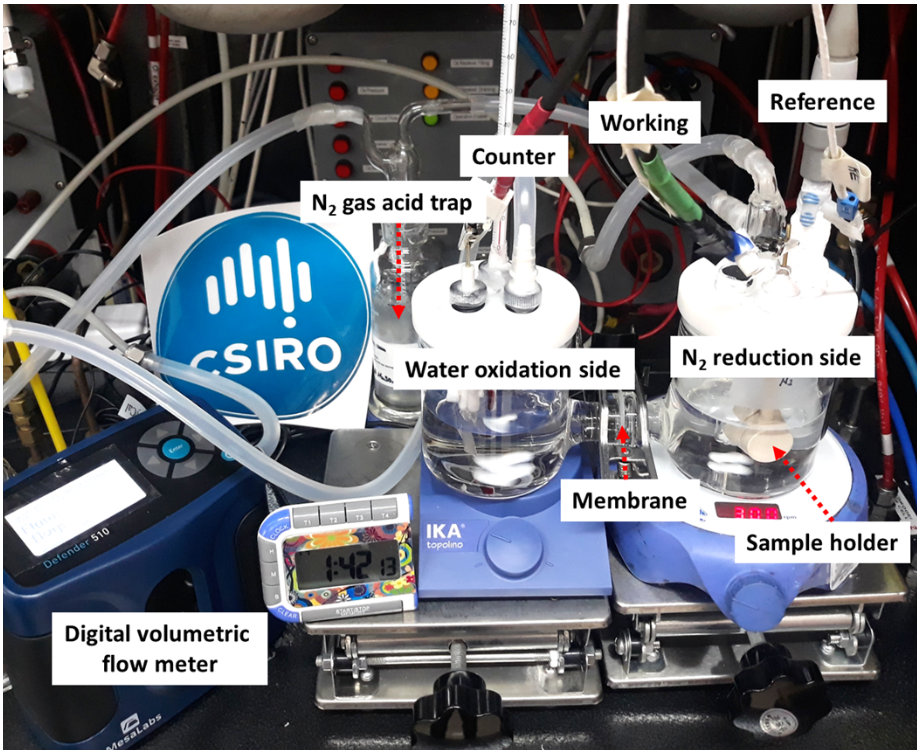

Figure S1. Image of an optimized glass H-type cell with a two-compartment chamber with a three-electrode configuration. The H-type cell consists of a working (ammonia synthesis side) and a counter (water oxidation reaction side) electrode chambers and separated by a Nafion 115 membrane. Pt gauze (1 cm x 1 cm,100 mesh, 99.9%, Aldrich) and Ag/AgCl, 3 M KCl were employed as the counter and reference electrodes, respectively.

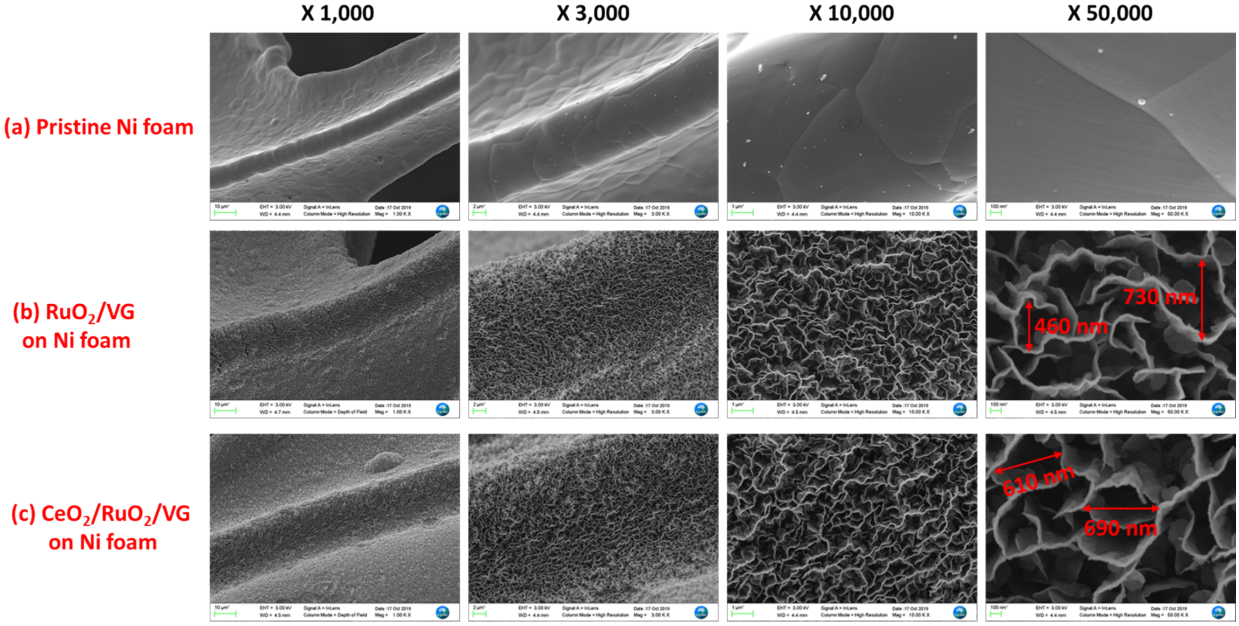

Figure S2. Additional FE-SEM images of (a) pristine Ni foam, (b) RuO_2/VG on Ni foam, and (c) CeO_2/RuO_2/VG on Ni foam.

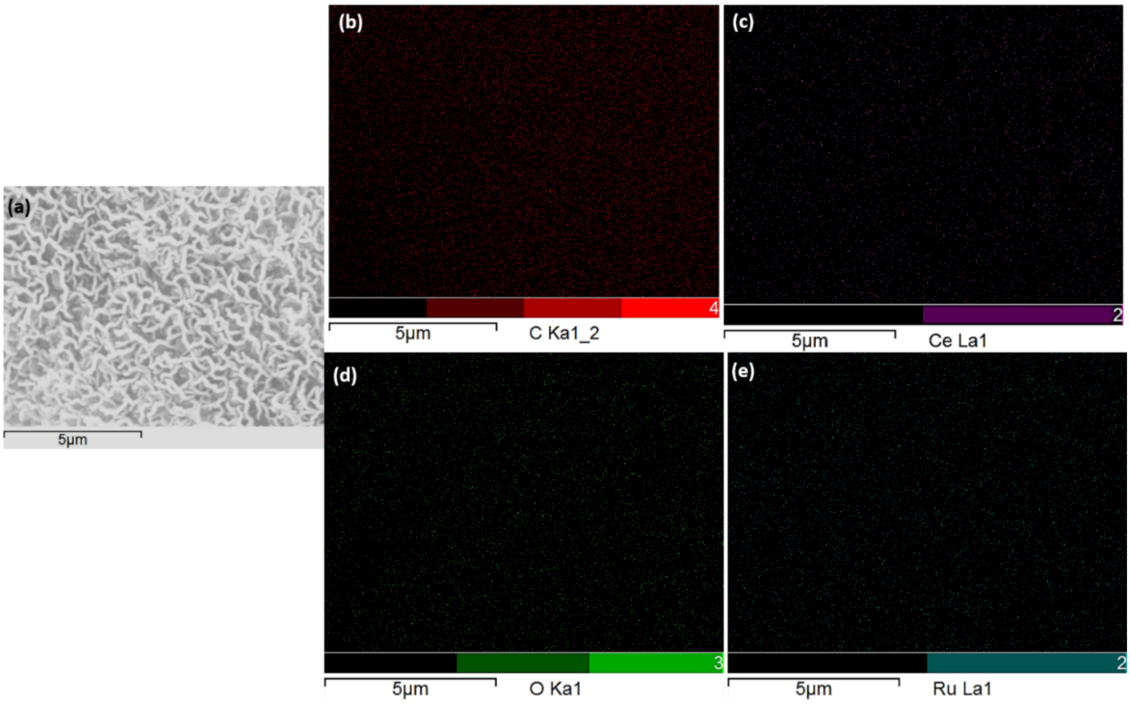

Figure S3. (a) BSE image with EDX element maps of (b) C, (c) Ce, (d) O, and (e) Ru of CeO_2/RuO_2/VG on Ni foam reveals the good and uniform coverage of VG, CeO_2 and RuO_2 is observed.

Table S1. Surface compositions as measured by XPS, expressed in atomic concentrations (%). Shown are mean values (+/- deviation) of two measurements per sample.

Sample	Ni foam		VG on Ni foam		RuO_2/VG on Ni foam		CeO_2/RuO_2/VG on Ni foam	
	Mean	*Dev.*	**Mean**	*Dev.*	**Mean**	*Dev.*	**Mean**	*Dev.*
C	**24.49**	*0.12*	**98.83**	*0.11*	**74.86**	*0.62*	**29.24**	*0.45*
O	**38.66**	*0.27*	**1.14**	*0.15*	**15.15**	*0.28*	**44.68**	*0.22*
N			**0.04**	*0.04*	**1.18**	*0.06*	**0.12**	*0.12*
Cl	**0.39**	*0.07*			**0.05**	*0.02*		
Ni	**36.45**	*0.21*						
Ru					**8.77**	*0.27*	**0.23**	*0.11*
Ce							**25.73**	*0.00*

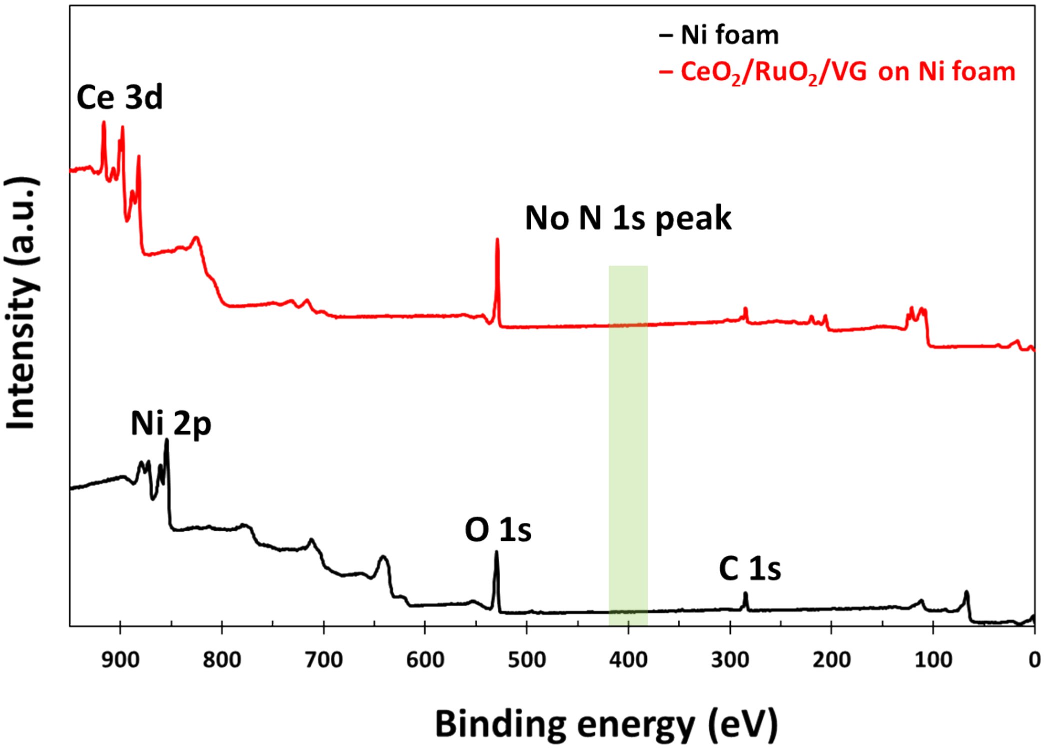

Figure S4. XPS wide-scan spectrum of $CeO_2/RuO_2/VG$ on Ni foam. XPS reveals that there is negligible presence of nitrogen affecting or contributing to the ammonia production from the samples.

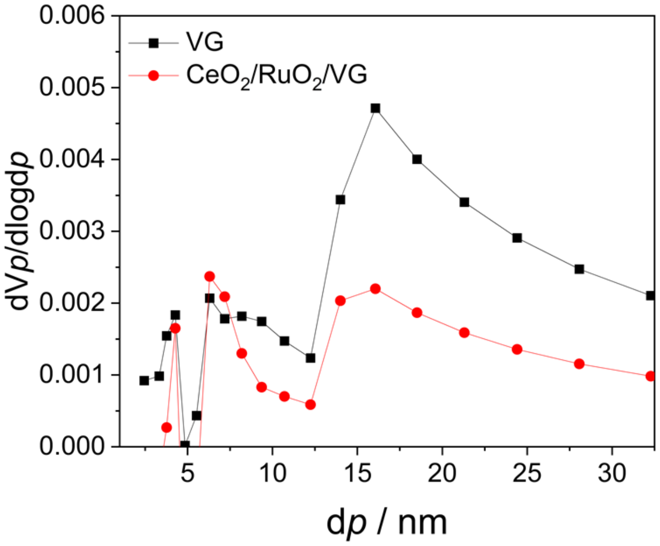

Figure S5. Brunauer-Emmett-Teller (BET) measurement (BEL JAPAN Inc., Japan) under N_2 adsorption/desorption isotherms at 77 K. Particle size distribution of VG and $CeO_2/RuO_2/VG$ on Ni foam.

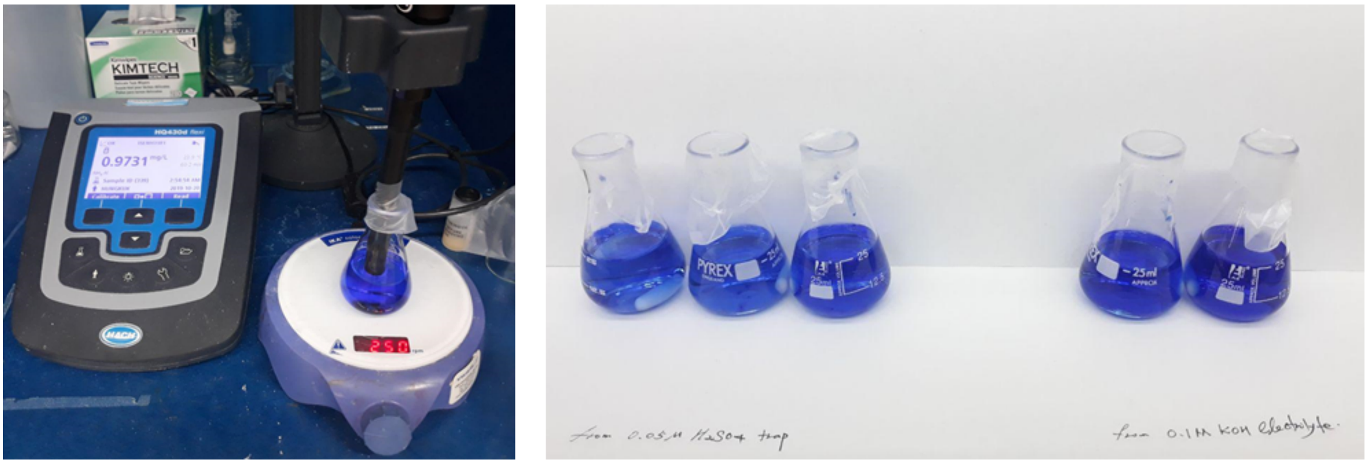

Figure S6. Ion-selective electrode (ISE) method of measuring ammonia contents. Photograph showing the one of a method which was used to measure the ammonia production rate.

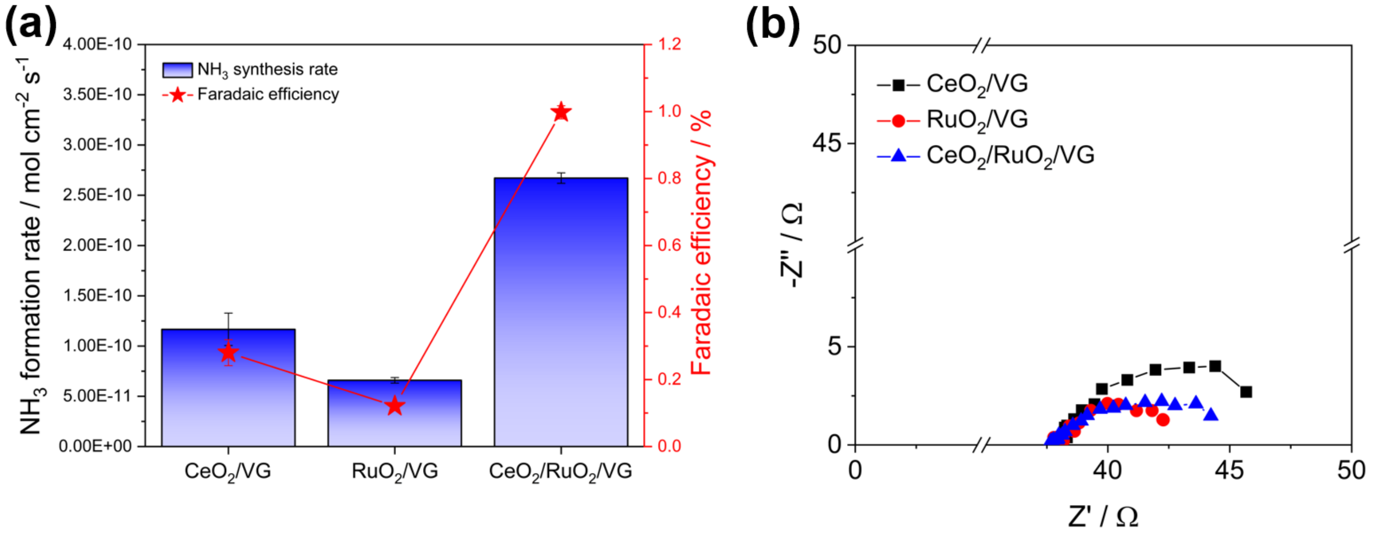

Figure S7. (a) NH_3 formation rates and Faradaic efficiencies of CeO_2/VG, RuO_2/VG and CeO_2/RuO_2/VG catalysts on Ni foam at -0.6 V vs. RHE in N_2-saturated 0.1 M KOH electrolyte. The NH_3 in the trap chamber was determined by indophenol-blue method. (b) Nyquist plots of CeO_2/VG, RuO_2/VG and CeO_2/RuO_2/VG catalysts during NRR at -0.6 V vs. RHE in N_2-saturated 0.1 M KOH.

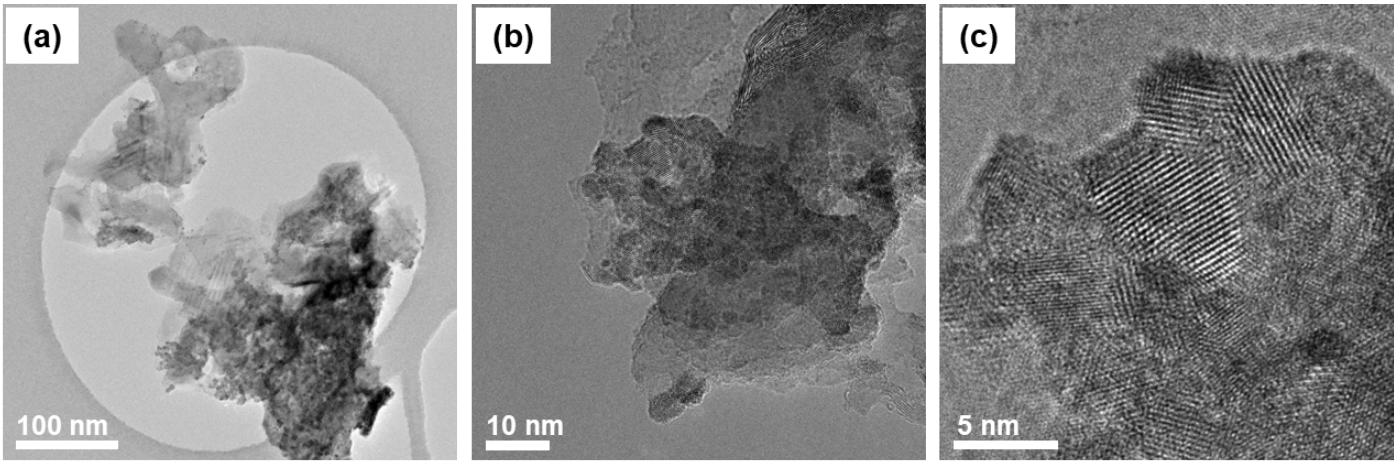

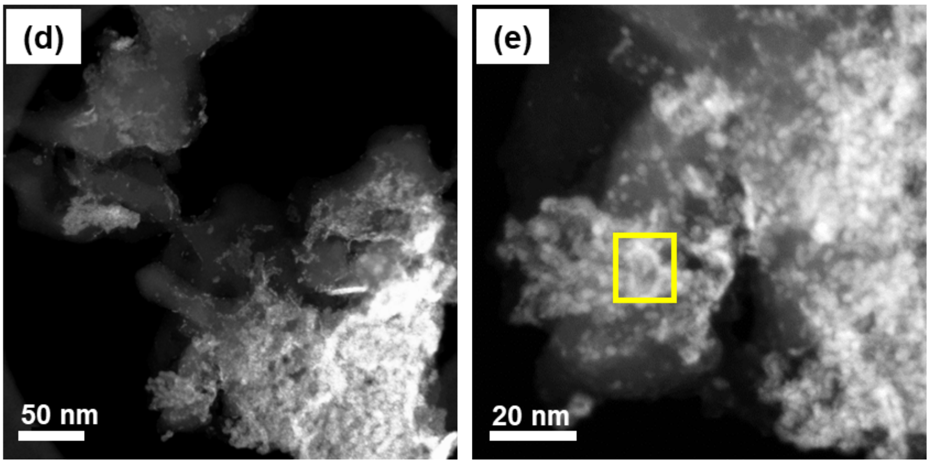

(f)

Elements	Atomic percent (%)
O	53.6
Ru	26.6
Ce	19.8

Figure S8. HR-TEM analysis of the CeO_2/RuO_2/VG catalysts after the long-term performance test. (a-c) reveals the HR-TEM images of CeO_2/RuO_2/VG catalysts. (d-e) shows the Revealing the HAADF-STEM images of CeO_2/RuO_2/VG. (f) Showing the elemental composition of CeO_2 and RuO_2 nanoparticles distributed on the vertical graphene sheets. Through the HR-TEM analysis, it can be noted that the CeO_2 and RuO_2 nanoparticles remained intact on the vertical graphene sheets and minimal chemical modification occurred for the CeO_2 and RuO_2 nanoparticles during the long-term performance test.

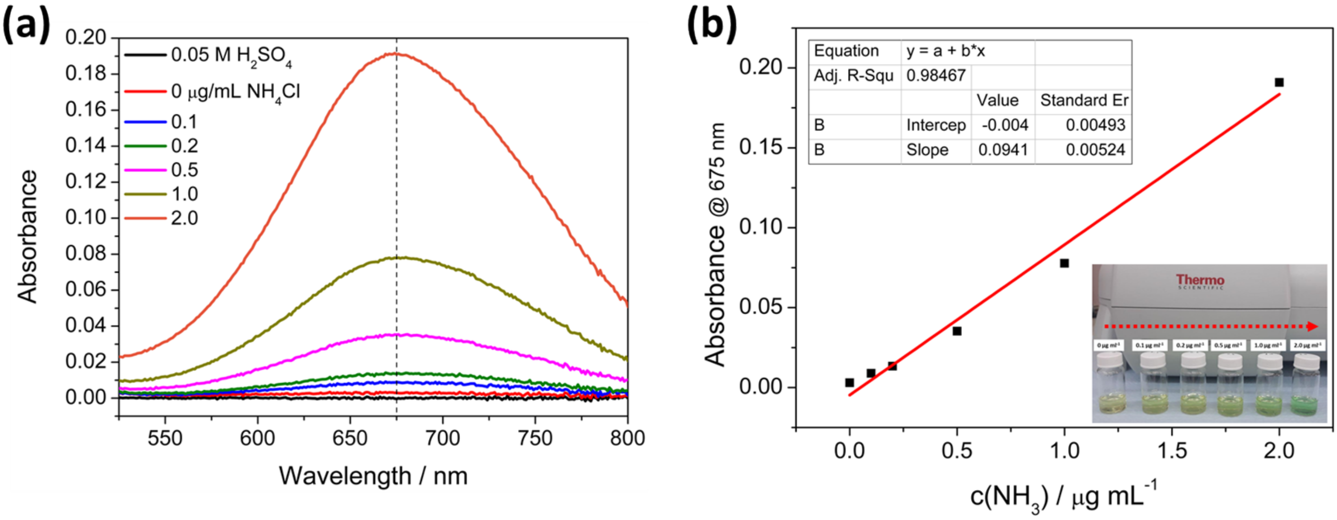

Equation	y = a + b*x		
Adj. R-Squ	0.98467		
		Value	Standard Er
B	Intercep	-0.004	0.00493
B	Slope	0.0941	0.00524

Figure S9. (a) UV-vis absorption spectra of indophenol blue method. (b) Calibration curves used for determining NH_4^+ ions (ammonia concentration) and distinctive colour change is observed depending on the concentrations of ammonia in this method.

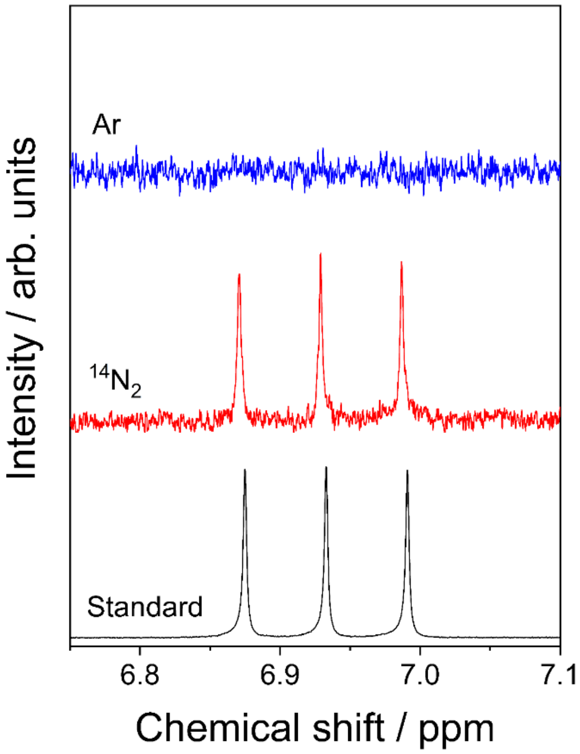

Figure S10. ^{1}H nuclear magnetic resonance (NMR) spectra were obtained from the durability test as per Fig. 6. The produced ammonia (NH_4^+ in 0.05M H_2SO_4) from the cathode chamber was identified under the $^{14}N_2$ experiment using a 900 MHz ^{1}H liquid-state nuclear magnetic resonance (^{1}H NMR) spectroscopy.

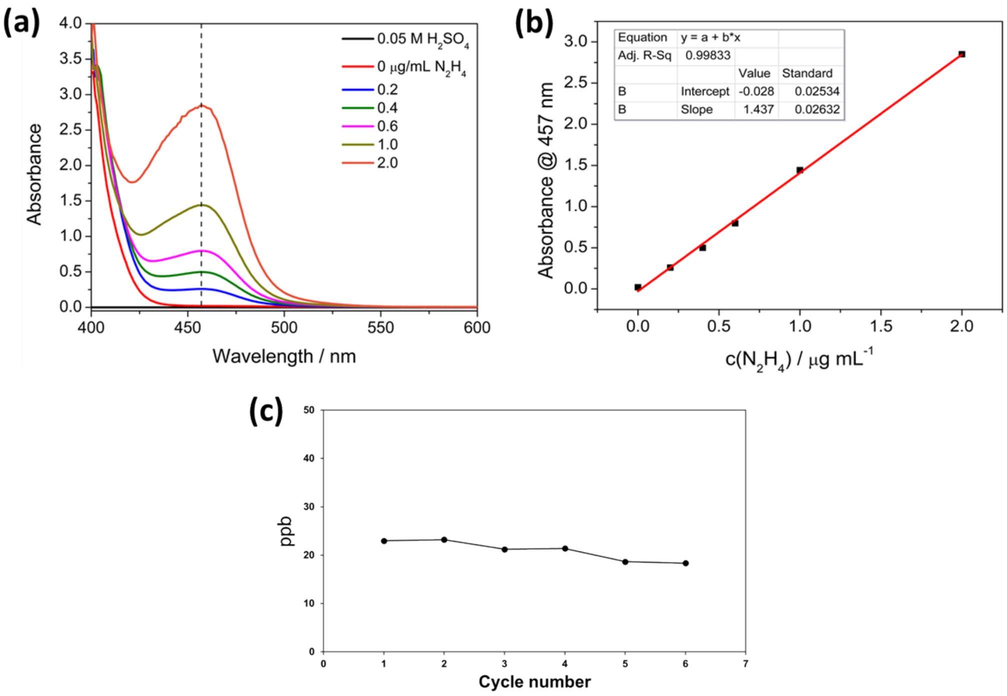

Figure S11. (a) UV-vis absorption spectra of Watt and Chrisp's method for detecting hydrazine (N_2H_4). (b) Calibration curves used for determining hydrazine concentration. (c) Hydrazine concentration curves during during all consecutive NRR cycle tests as per Fig. 6.

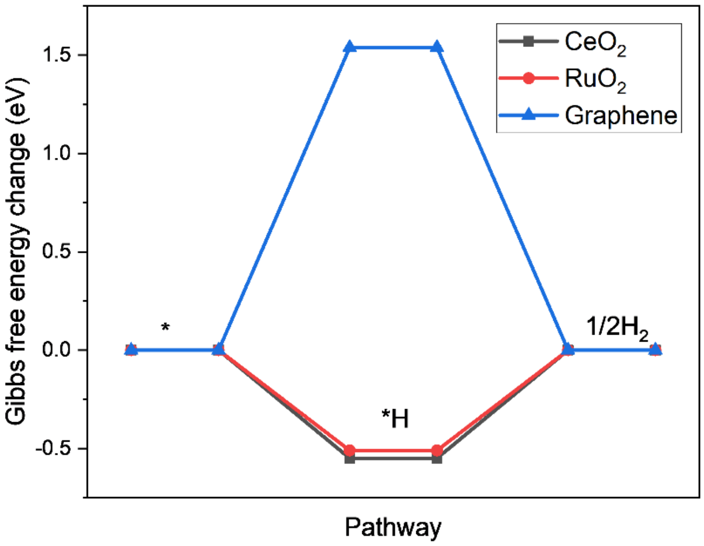

Figure S12. DFT calculation of HER process using CeO_2 and RuO_2 and Graphene surfaces.

Table S2. Table showing the recent literatures on electrochemical production of ammonia.

Catalyst	**Active area**	**Membrane**	**Electrolyte**	**T**	**Applied potential**	**Current density**	**NH_3 yield**	**FE%**	**Long-term**	**Ref**
CeO_2/RuO_2 on vertical graphene	0.785 cm^2	Nafion 115	0.1 M KOH	Room Temp.	-0.6 V vs. RHE	~ -25 mA/cm^2	50.56 µg/h mg_{cat} 1.11×10^{-10} mol $s^{-1}cm^{-2}$	2.96%	36 hr	**This work**
N-doped Cu SA	1 cm^2	Nafion 211	0.1 M KOH	AT	-0.35 V vs. RHE	-0.5 mA/cm^2	53.3 µg/h mg_{cat}	13.8%	~14 hr	**10**
PdRu tripods	0.25 cm^2	Nafion 211	0.1 M KOH	25ºC	-0.2 V vs. RHE	-6.5 mA/cm^2	37.23 µg/h mg_{cat} 11.9 µg/h cm^2	1.85%	20 hr	**11**
SA-Mo/NPC	-	Nafion 117	0.1 M KOH	Room Temp.	-0.3 V vs. RHE	~ -2.5 mA/cm^2	34 µg/h mg_{cat}	14.6%	~14 hr	**12**
$Pd_{0.2}Cu_{0.8}$/rGO	1 cm^2	Nafion 211	0.1 M KOH	Room Temp.	-0.2 V vs. RHE	-1 mA/cm^2	2.8 µg/h mg_{cat}	~1%	-	**13**
C-ZIF	0.245 cm^2	Half-cell	0.1 M KOH	Room Temp.	-0.3 V vs. RHE	-0.2 mA/cm^2	9.4×10^{-10} mol/s cm^2 (3.4×10^{-6} mol/h cm^2)	10.2%	9 hr	**14**

Catalyst	Active area	Membrane	Electrolyte	T	Applied potential	Current density	NH_3 yield	FE%	Long-term	Ref
Fe_3Mo_3C/C	0.3 cm^2	Nafion 211	1 M KOH	25ºC 1 / 7 bar	-0.5 V vs. RHE	~ -133 mA/cm^2	13.1 µg/h cm^2 at -0.5 V 0.1 MPa	0.05%	-	15
							13.55 µg/h cm^2 at 0.7 MPa at -0.025 V	14.74%	-	
Ru Li on Ag	-	Nafion 117	0.1 M KOH	20ºC	-1 ~ -2.5 V vs. RHE	<-10 µA/cm^2		<0.01%	~14 hr	16
			0.2 M LiClO4			<-1 mA/cm^2	0.6-0.7 µmol/h cm^2	<10%	-	
Rh nanosheet	0.25 cm^2	Nafion 211	0.1 M KOH	Room Temp.	-0.2 V vs. RHE	~ -20 mA/cm^2	23.88 µg/h mg_{cat}	0.217%	30 hr	17
30% Fe_2O_3-CNT	-	Nafion	0.5 M KOH	20ºC	-2.0 V vs. Ag/AgCl	-7 mA/cm^2	1.06 x 10^{-11} mol/s cm^2	0.164%	24 hr	18
Au THH	1 cm^2	Nafion 211	0.1 M KOH	25ºC	-0.2 V vs. RHE	<-1 mA/cm^2	1.648 µg/h mg_{cat}	4%	18 hr	19
Ru nanoparticles	-	Nafion 115	0.1 M HCl	25ºC	-0.15 V vs. RHE	~ -5 mA/cm^2	24.88 µg/h mg_{cat}	0.35%	24 hr	20

Mesoporous RhRu film on Ni foam	1.5 cm^2	Nafion 211	0.1 M Na_2SO_4	25ºC	-0.05 V vs. RHE	~ 0.01 mA/cm^2	30.28 µg/h mg$_{cat}$	28.33%	20 hr	[21]

Catalyst	Active area	Membrane	Electrolyte	T	Applied potential	Current density	NH_3 yield	FE%	Long-term	Ref
TiO_2 nanoarray	0.5 cm^2	Nafion 117	0.05 M H_2SO_4 with PEG	Room Temp.	-0.3 V vs. RHE	<-0.5 mA/cm^2	1.07 µmol/h cm^2	32.13%	10 hr	[22]
Cu coated GDE	6 cm^2	Anion exchange membrane	0.32 M KOH	Room Temp.	-0.3 V vs. RHE	-0.25 mA/cm^2	0.86 nmol/s cm^2	18%	-	[23]
NiPS3 nanosheet	1 cm^2	Nafion	0.1 M Na_2SO_4	Room Temp.	-0.4 V vs. RHE	~ -1 mA/cm^2	118 µg/h mg$_{cat}$	17%	10 hr	[24]

References

(1) Seo, D. H.; Rider, A. E.; Han, Z. J.; Kumar, S.; Ostrikov, K. (Ken). Plasma Break-Down and Re-Build: Same Functional Vertical Graphenes from Diverse Natural Precursors. *Advanced Materials* **2013**, *25* (39), 5638–5642. https://doi.org/10.1002/adma201301510.

(2) Watt, G. W.; Chrisp, J. D. Spectrophotometric Method for Determination of Hydrazine. *Anal. Chem.* **1952**, *24* (12), 2006–2008. https://doi.org/10.1021/ac60072a044.

(3) Perdew, J. P.; Ernzerhof, M.; Burke, K. Rationale for Mixing Exact Exchange with Density Functional Approximations. *J. Chem. Phys.* **1996**, *105* (22), 9982–9985. https://doi.org/10.1063/1.472933.

(4) Kresse, G.; Furthmüller, J. Efficient Iterative Schemes for Ab Initio Total-Energy Calculations Using a Plane-Wave Basis Set. *Phys. Rev. B* **1996**, *54* (16), 11169–11186. https://doi.org/10.1103/PhysRevB.54.11169.

(5) Kresse, G.; Furthmüller, J. Efficiency of Ab-Initio Total Energy Calculations for Metals and Semiconductors Using a Plane-Wave Basis Set. *Computational Materials Science* **1996**, *6* (1), 15–50. https://doi.org/10.1016/0927-0256(96)00008-0.

(6) Grimme, S. Semiempirical GGA-type density functional constructed with a long-range dispersion correction. *Journal of Computational Chemistry* **2006**, *27* (15), 1787–1799. https://doi.org/10.1002/jcc.20495.

(7) Montoya, J. H.; Tsai, C.; Vojvodic, A.; Nørskov, J. K. The Challenge of Electrochemical Ammonia Synthesis: A New Perspective on the Role of Nitrogen Scaling Relations. *ChemSusChem* **2015**, *8* (13), 2180–2186. https://doi.org/10.1002/cssc.201500322.

(8) Medford, A. J.; Wellendorff, J.; Vojvodic, A.; Studt, F.; Abild-Pedersen, F.; Jacobsen, K. W.; Bligaard, T.; Nørskov, J. K. Assessing the Reliability of Calculated Catalytic Ammonia Synthesis Rates. *Science* **2014**, *345* (6193), 197–200. https://doi.org/10.1126/science.1253486.

(9) Singh, A. R.; Rohr, B. A.; Statt, M. J.; Schwalbe, J. A.; Cargnello, M.; Nørskov, J. K. Strategies toward Selective Electrochemical Ammonia Synthesis. *ACS Catal.* **2019**, *9* (9), 8316–8324. https://doi.org/10.1021/acscatal.9b02245.

(10) Zang, W.; Yang, T.; Zou, H.; Xi, S.; Zhang, H.; Liu, X.; Kou, Z.; Du, Y.; Feng, Y. P.; Shen, L.; Duan, L.; Wang, J.; Pennycook, S. J. Copper Single Atoms Anchored in Porous Nitrogen-Doped Carbon as Efficient PH-Universal Catalysts for the Nitrogen Reduction Reaction. *ACS Catal.* **2019**, 10166–10173. https://doi.org/10.1021/acscatal.9b02944.

(11) Wang, H.; Li, Y.; Li, C.; Deng, K.; Wang, Z.; Xu, Y.; Li, X.; Xue, H.; Wang, L. One-Pot Synthesis of Bi-Metallic PdRu Tripods as an Efficient Catalyst for Electrocatalytic Nitrogen Reduction to Ammonia. *J. Mater. Chem. A* **2019**, *7* (2), 801–805. https://doi.org/10.1039/C8TA09482A.

(12) Han, L.; Liu, X.; Chen, J.; Lin, R.; Liu, H.; Lü, F.; Bak, S.; Liang, Z.; Zhao, S.; Stavitski, E.; Luo, J.; Adzic, R. R.; Xin, H. L. Atomically Dispersed Molybdenum Catalysts for Efficient Ambient Nitrogen Fixation. *Angew. Chem. Int. Ed.* **2019**, *58* (8), 2321–2325. https://doi.org/10.1002/anie.201811728.

(13) Shi, M.-M.; Bao, D.; Li, S.-J.; Wulan, B.-R.; Yan, J.-M.; Jiang, Q. Anchoring PdCu Amorphous Nanocluster on Graphene for Electrochemical Reduction of N2 to NH3 under Ambient Conditions in Aqueous Solution. *Advanced Energy Materials* **2018**, *8* (21), 1800124. https://doi.org/10.1002/aenm.201800124.

(14) Mukherjee, S.; Cullen, D. A.; Karakalos, S.; Liu, K.; Zhang, H.; Zhao, S.; Xu, H.; More, K. L.; Wang, G.; Wu, G. Metal-Organic Framework-Derived Nitrogen-Doped Highly Disordered Carbon for Electrochemical Ammonia Synthesis Using N_2 and H_2O in Alkaline Electrolytes. *Nano Energy* **2018**, *48*, 217–226. https://doi.org/10.1016/j.nanoen.2018.03.059.

(15) Cheng, H.; Cui, P.; Wang, F.; Ding, L.-X.; Wang, H. High Efficiency Electrochemical Nitrogen Fixation Achieved with a Lower Pressure Reaction System by Changing the Chemical Equilibrium. *Angew. Chem. Int. Ed.* **2019**, 41.

(16) Andersen, S. Z.; Čolić, V.; Yang, S.; Schwalbe, J. A.; Nielander, A. C.; McEnaney, J. M.; Enemark-Rasmussen, K.; Baker, J. G.; Singh, A. R.; Rohr, B. A.; Statt, M. J.; Blair, S. J.; Mezzavilla, S.; Kibsgaard, J.; Vesborg, P. C. K.; Cargnello, M.; Bent, S. F.; Jaramillo, T. F.; Stephens, I. E. L.; Nørskov, J. K.; Chorkendorff, I. A Rigorous Electrochemical Ammonia Synthesis Protocol with Quantitative Isotope Measurements. *Nature* **2019**, *570* (7762), 504–508. https://doi.org/10.1038/s41586-019-1260-x.

(17) Liu, H.-M.; Han, S.-H.; Zhao, Y.; Zhu, Y.-Y.; Tian, X.-L.; Zeng, J.-H.; Jiang, J.-X.; Xia, B. Y.; Chen, Y. Surfactant-Free Atomically Ultrathin Rhodium Nanosheet Nanoassemblies for Efficient Nitrogen Electroreduction. *J. Mater. Chem. A* **2018**, *6* (7), 3211–3217. https://doi.org/10.1039/C7TA10866D.

(18) Chen, S.; Perathoner, S.; Ampelli, C.; Mebrahtu, C.; Su, D.; Centi, G. Room-Temperature Electrocatalytic Synthesis of NH_3 from H_2O and N_2 in a Gas–Liquid–Solid Three-Phase Reactor. *ACS Sustainable Chem. Eng.* **2017**, *5* (8), 7393–7400. https://doi.org/10.1021/acssuschemeng.7b01742.

(19) Bao, D.; Zhang, Q.; Meng, F.-L.; Zhong, H.-X.; Shi, M.-M.; Zhang, Y.; Yan, J.-M.; Jiang, Q.; Zhang, X.-B. Electrochemical Reduction of N_2 under Ambient Conditions for Artificial N_2 Fixation and Renewable Energy Storage Using N_2/NH_3 Cycle. *Adv. Mater.* **2017**, *29* (3), 1604799. https://doi.org/10.1002/adma.201604799.

(20) Zhao, L; Zhao, J; Zhao, J; Zhang, L; Wu, D; Wang, H; Li, J; Ren, X; Wei, Q. Artificial N_2 fixation to NH_3 by electrocatalytic Ru NPs at low overpotential. *Nanotechnology* **2020**, 31, 29LT01.

(21) Wang, Z; Tian, W; Dai, Z; Zhou, T; Mao, Q; Xu, Y; Li, X; Wang, L; Wang, H. Bimetallic mesoporous RhRu film for electrocatalytic nitrogen reduction to ammonia. *Inorg. Chem. Front*. **2021**, 8, 4276.

(22) Guo, Y; Gu, J; Zhang, R; Zhang, S; Li, Z; Zhao, Y; Huang, Z; Fan, J; Chen, Z; Zhi, C. Molecular crowding effect in aqueous electrolytes to suppress hydrogen reduction reaction and enhance electrochemical nitrogen reduction. *Advanced Energy Materials*. **2021**, 11, 2101699.

(23) Kani, N.C.; Prajapati, A; Collins, B.A; Goodpaster, J.D; Singh, M.R. Competing effects of pH, cation identity, H2O saturation, and N2 concentration on the activity and selectivity of electrochemical reduction of N2 to NH3 on electrodeposited Cu at ambient conditions. *ACS Catal*. **2020**, 10, 14592-14603.

(24) Vedhanarayanan, B; Chiu, C.-C; Regner, J.; Sofer, Z; Lakshmi, K.C.S; Lin, J.-Y.; Lin, T.-W. Highly exfoliated NiPS3 nanosheets as efficient electrocatalyst for high yield ammonia production. *Chem. Eng. J.* **2022**, 430, 132649.